AUTHOR(S):

Sugahara, Michihiro; Nakane, Takanori; Masuda, Tetsuya; Suzuki, Mamoru; Inoue, Shigeyuki; Song, Changyong; Tanaka, Rie; … Numata, Keiji; Nango, Eriko; Iwata, So

www.nature.com/scientificreports

SCIENTIFIC REP🜨RTS

Hydroxyethyl cellulose matrix applied to serial crystallography

Michihiro Sugahara[1], Takanori Nakane[2], Tetsuya Masuda[1,3], Mamoru Suzuki[1,4], Shigeyuki Inoue[1,5], Changyong Song[6], Rie Tanaka[1], Toru Nakatsu[7], Eiichi Mizohata[8], Fumiaki Yumoto[9], Kensuke Tono[10], Yasumasa Joti[10], Takashi Kameshima[10], Takaki Hatsui[1], Makina Yabashi[1], Osamu Nureki[2], Keiji Numata[11], Eriko Nango[1] & So Iwata[1,12]

Serial femtosecond crystallography (SFX) allows structures of proteins to be determined at room temperature with minimal radiation damage. A highly viscous matrix acts as a crystal carrier for serial sample loading at a low flow rate that enables the determination of the structure, while requiring consumption of less than 1 mg of the sample. However, a reliable and versatile carrier matrix for a wide variety of protein samples is still elusive. Here we introduce a hydroxyethyl cellulose-matrix carrier, to determine the structure of three proteins. The *de novo* structure determination of proteinase K from single-wavelength anomalous diffraction (SAD) by utilizing the anomalous signal of the praseodymium atom was demonstrated using 3,000 diffraction images.

Serial femtosecond crystallography (SFX) using ultrashort pulses from X-ray free-electron lasers (XFELs) can overcome typical radiation damage to protein crystals via the "diffraction-before-destruction" approach[1–7]. This has been used to obtain crystal structures of interesting proteins at room temperature[8–18]. Liquid jet injection of small protein crystals with continuous flow at relatively high speed (~10 m sec^{-1}) is frequently exploited for serial sample loading[19], consuming 10~100 mg of the sample. To reduce sample consumption, micro-extrusion techniques of specimens using viscous media such as a lipidic cubic phase (LCP)[20], grease[21], Vaseline (petroleum jelly)[22] and agarose[23] have been developed. These media can maintain a stable stream at a lower flow rate of 0.02~0.5 μl min^{-1} allowing sample consumption of less than ~1 mg. More recently, synchrotron-based serial crystallography has also been developed[22, 24, 25], demonstrating that the sample loading technique with a viscous media becomes even more important in serial crystallography. This method with viscous media is technically simple, but some media produce stronger X-ray scattering that increase background noise. For data collection from small crystals (~1 μm), at atomic resolution, and *de novo* phasing with weak anomalous signals, a crystal carrier with low background scattering is essential to improve the signal-to-noise ratio[23]. To reduce background scattering from the carrier media, we introduced a hyaluronic acid matrix in SFX[26]. At the SPring-8 Angstrom Compact Free Electron Laser (SACLA)[27], we operate an injector system under a helium atmosphere at 1 atm during micro-extrusion of the matrices[28]. However, hyaluronic acid matrix is strongly adhesive, resulting in frequent clogging of the sample-vacuum nozzle which acts as a sample catcher[22] in our injector system. In addition, the general adaptability of hydrogel matrices to *de novo* phasing with heavy atoms is still unclear.

[1]RIKEN SPring-8 Center, 1-1-1 Kouto, Sayo-cho, Sayo-gun, Hyogo, 679-5148, Japan. [2]Department of Biological Sciences, Graduate School of Science, The University of Tokyo, 7-3-1 Hongo, Bunkyo-ku, Tokyo, 113-0033, Japan. [3]Division of Food Science and Biotechnology, Graduate School of Agriculture, Kyoto University, Gokasho, Uji, Kyoto, 611-0011, Japan. [4]Institute for Protein Research, Osaka University, 3-2 Yamadaoka, Suita, Osaka, 565-0871, Japan. [5]Department of Cell Biology and Anatomy, Graduate School of Medicine, The University of Tokyo, 7-3-1 Hongo, Bunkyo-ku, Tokyo, 113-0033, Japan. [6]Department of Physics, POSTECH, Pohang, 37673, Republic of Korea. [7]Department of Structural Biology, Graduate School of Pharmaceutical Sciences, Kyoto University, 46-29 Yoshida Shimoadachi-cho, Sakyo-ku, Kyoto, 606-8501, Japan. [8]Department of Applied Chemistry, Graduate School of Engineering, Osaka University, 2-1 Yamadaoka, Suita, Osaka, 565-0871, Japan. [9]Structural Biology Research Center, KEK High Energy Accelerator Research Organization, Tsukuba, Ibaraki, 305-0801, Japan. [10]Japan Synchrotron Radiation Research Institute, 1-1-1 Kouto, Sayo-cho, Sayo-gun, Hyogo, 679-5198, Japan. [11]Enzyme Research Team, Biomass Engineering Research Division, RIKEN Center for Sustainable Resource Science, Hirosawa, Wako-shi, Saitama, 351-0198, Japan. [12]Department of Cell Biology, Graduate School of Medicine, Kyoto University, Yoshidakonoe-cho, Sakyo-ku, Kyoto, 606-8501, Japan. Correspondence and requests for materials should be addressed to M.S. (email: msuga@spring8.or.jp)

Here we introduce hydroxyethyl cellulose (cellulose matrix) for serial sample loading. We demonstrate the cellulose matrix as a protein carrier for SFX using small and large sized crystals ($1 \times 1 \times 1$ to $20 \times 20 \times 30\,\mu m$). In addition, we demonstrate the successful *de novo* phasing in SFX by applying praseodymium (Pr)-SAD, single-isomorphous replacement (SIR) and SIR with anomalous scattering (SIRAS) phasing to determine the structure of proteinase K. Furthermore, to reduce background scattering, a novel grease matrix, Super Lube nuclear grade grease (nuclear grease), was introduced in this study.

Results and Discussion

Crystal structures for lysozyme and thaumatin.
We performed SFX experiments using femtosecond X-ray pulses from SACLA. Using lysozyme ($1 \times 1 \times 1\,\mu m$) and thaumatin ($2 \times 2 \times 4\,\mu m$) crystals (Supplementary Fig. 1a,b) dispersed in a cellulose matrix, we were able to collect 100,000–150,000 images in approximately 60–80 min at a wavelength of 1.24 Å (Table 1). At a flow rate of 0.43 and 0.47 μl min^{-1}, a total sample volume of about 30–40 μl was used with a crystal number density of 5.8×10^8 crystals ml^{-1} for lysozyme, and 4.3×10^8 crystals ml^{-1} for thaumatin. We indexed and integrated 30,000–40,000 images for both the lysozyme (space group $P4_32_12$) and thaumatin (space group $P4_12_12$) crystals. The lysozyme and thaumatin crystals yielded data sets at 1.8-Å and 1.55-Å resolution with a completeness of 100% and a CC$_{1/2}$ of 0.992 and 0.988, respectively. We determined and refined the crystal structures of lysozyme [Protein Data Bank (PDB) ID: 5wr9] and thaumatin (PDB ID: 5wr8) at 1.8-Å and 1.55-Å resolution (Fig. 1a,b), respectively. For the larger lysozyme crystals of the size $20 \times 20 \times 30\,\mu m$, the X-ray wavelength was kept at 0.95 Å. The microcrystals were used to acquire data sets at 1.45-Å resolution with a completeness of 100% and a CC$_{1/2}$ of 0.995 (PDB ID: 5wra, Table 1).

In this study, 16% (*w/v*) and 22% (*w/v*) cellulose matrices were used for the small sized lysozyme ($1 \times 1 \times 1\,\mu m$) and thaumatin ($2 \times 2 \times 4\,\mu m$) crystals, respectively. The cellulose matrix with randomly oriented crystals was extruded through an injector nozzle with an inner diameter (i.d.) of 50 μm. On the other hand, for the larger lysozyme crystals ($20 \times 20 \times 30\,\mu m$), an 11% (*w/v*) cellulose matrix was extruded through a 130-μm-i.d. nozzle. The cellulose matrix formed a stable flow for all protein samples (an example: Supplementary Fig. 2a). The matrix at low cellulose concentrations (less than ~5%) cannot be extruded from our injector system as a continuous sample column. On the other hand, a matrix at a cellulose concentration (~30%) becomes too hard for micro-extrusion. The cellulose concentration therefore was preferably ~10–20%. The sample preparation in our technique can be performed by simply mixing with matrix medium. Although the medium mixing technique using a syringe coupler may prevent crystal dehydration[23, 29], the technique could cause mechanical damage to brittle crystals by physical contact between the crystals and the coupler interior surface, resulting in a deterioration of diffraction quality. In such cases, a simple, quick mixing with a spatula on a glass slide[21] would be better to preserve the crystals. The cellulose matrix has lower background scattering (Supplementary Fig. 3a) compared to the conventional grease matrix, the synthetic grease Super Lube (Supplementary Fig. 3b) generated diffuse scatterings in the resolution range of 4–5 Å, and LCP[14] (Fig. 2), while the cellulose matrix gives a slightly higher background scattering in the resolution range of ~3.5–2.5 Å. There were no significant differences between cellulose and hyaluronic acid matrices[26], suggesting that polysaccharide hydrogels tend to have lower background scattering. However, the cellulose matrix is less adhesive than the hyaluronic acid matrix and prevents clogging of the sample-vacuum nozzle as a sample catcher[22] (Supplementary Fig. 2) and adhesion of the matrix to the injector nozzle surface in our injector system. In addition, hyaluronic acid is more expensive compared to hydroxyethyl cellulose, up to ~1,000 times the price per gram. Hydrogels, LCP and Vaseline can be extruded as a continuous column with an approximately same diameter as a 50-μm-i.d. (or less) injector nozzle size. On the other hand, grease matrix tends to produce a column larger than the nozzle i.d. A sample column with a smaller diameter (~50 μm) contributes to the reduction of sample consumption and background scattering from the matrix[26]. A matrix with low background scattering is important to collect a high-resolution data set from ~1 μm (or less) crystals.

De novo phasing.
Crystallographic phasing for routine structure determination remains a challenge in SFX. In this study, using the cellulose matrix, we attempted the *de novo* phasing of proteinase K. We collected ~180,000 images from the microcrystals (size $4 \times 4 \times 4$–$5 \times 5 \times 7\,\mu m$) of Pr-derivatized proteinase K (Supplementary Fig. 1c) at a wavelength of 1.24 Å (Table 1). We successfully indexed and integrated approximately 31,000 images in space group $P4_32_12$. The dataset extended to 1.5-Å resolution with a completeness of 100% and a CC$_{1/2}$ of 0.990. The overall $<I/\sigma(I)>$ of the merged observations was 10.2. Substructure determination and phasing were performed by *SHELXD* and *SHELXE*[30]. We succeeded in locating two Pr ions in the asymmetric unit and could solve the substructure at 2.0-Å resolution, but not at 2.2-Å resolution. The two Pr-binding sites were identical to those of the calcium ions in the native structure (Fig. 3), indicating that the two calcium atoms were replaced by the Pr atoms[31]. The coordinates of the heavy atoms were employed for both the refinement and the phase calculation at 1.8-Å resolution in *SHEXLE*. A polyalanine model of proteinase K was automatically traced by *SHELXE*. Subsequently, 99% (277 of 279 residues) of the structure was automatically modelled with side chains by *Buccaneer*[32]. Finally, we refined the structure at 1.5-Å resolution to an R/R_{free} of 17.6/19.3% (PDB ID: 5wrc). The expected magnitude of the anomalous signal ($<|\Delta F_{ano}|>/<|F|>$) is ~4.8% at 10 keV based on the formula in Hendrickson & Teeter[33] and Dauter *et al.*[34].

We found that 3,000 indexed images were sufficient for SAD phasing of proteinase K crystals. In this phasing, we used the first 3,000 of 30,930 indexed images, without deliberate selection of the best images. *SHELXD* located only one Pr atom in the asymmetric unit, when 3,000 indexed images were used. A polyalanine model from *SHELXE* at 1.7-Å resolution was completed in *Buccaneer*. We obtained 99% of the complete model. The final anomalous difference Fourier maps using 3,000 images in Fig. 3 display significant anomalous peak heights (17.1 and 11.2σ, obtained from *ANODE*[35]) of the two Pr atoms.

Protein	Lysozyme			Thaumatin
Carrier	16% cellulose	11% cellulose	Nuclear grease	22% cellulose
Crystal density (crystals/ml)	5.8×10^8	1.7×10^7	2.4×10^8	4.3×10^8
Crystal size (μm)	$1 \times 1 \times 1$	$20 \times 20 \times 30$	$5 \times 5 \times 5$	$2 \times 2 \times 4$
Nozzle size (μm)	50	130	100	50
Flow rate (μl/min)	0.43	0.75	0.42	0.47
Data collection				
wavelength (Å)	1.24	0.95	1.77	1.24
Space group	$P4_32_12$	$P4_32_12$	$P4_32_12$	$P4_12_12$
Unit-cell parameter				
$a = b$ (Å)	80.0	79.6	79.6	58.5
c (Å)	38.4	38.3	38.2	151.6
Number of collected images	149,938	107,856	105,769	101,383
Number of hits	41,575	58,321	30,929	55,751
Number of indexed images	29,593	40,787	19,271	43,350
Indexing rate from hits (%)	71.2	69.9	62.3	77.8
Number of merged images	29,593	40,787	19,271	43,350
Number of total reflections	4,823,284	21,187,517	3,440,102	24,822,961
Number of unique reflections	12,068	22,415	8,750	38,328
Resolution range (Å)	30–1.8 (1.86–1.80)	30–1.45 (1.50–1.45)	30–2.0 (2.07–2.00)	30–1.55 (1.60–1.55)
Completeness (%)	100 (100)	100 (100)	100 (100)	100 (100)
Multiplicity	399.7 (283.0)	945.2 (677.3)	393.2 (81.9)	647.6 (668.5)
R_{split} (%)[†]	7.1 (51.0)	5.1 (50.4)	8.0 (53.0)	8.6 (33.4)
$CC_{1/2}$	0.992 (0.764)	0.995 (0.735)	0.988 (0.654)	0.988 (0.760)
$<I/\sigma(I)>$	10.2 (2.2)	13.4 (2.2)	10.5 (2.0)	7.7 (2.0)
Total amounts of protein used (mg)	0.7	0.9	0.5	0.5
Refinement				
R/R_{free} (%)	17.5/18.4	18.1/19.6	18.1/20.2	12.7/15.1
R.m.s. deviations				
Bond lengths (Å)	0.008	0.007	0.008	0.006
Bond angles (°)	1.059	1.071	1.070	0.984
PDB code	5wr9	5wra	5wrb	5wr8

Protein	proteinase K				
Carrier	16% cellulose (Pr)			16% cellulose (native)	
Crystal density (crystals/ml)		9.3×10^7		4.9×10^7	
Crystal size (μm)		$4 \times 4 \times 4$–$5 \times 5 \times 7$		$8 \times 8 \times 8$–$12 \times 12 \times 12$	
Nozzle size (μm)		50		110	
Flow rate (μl/min)		0.47		0.38	
Data collection					
wavelength (Å)		1.24		0.95	
Space group		$P4_32_12$		$P4_32_12$	
Unit-cell parameter					
$a = b$ (Å)		68.6		68.3	
c (Å)		108.8		108.4	
Number of collected images		180,000		145,000	
Number of hits		40,503		59,246	
Number of indexed images		30,930		47,503	
Indexing rate from hits (%)		76.4		80.1	
Number of merged images	30,000	3,000	1,000	32,000	1,000
Number of total reflections	16,961,902	1,540,467	520,503	18,624,772	545,845
Number of unique reflections	42,391	42,386	42,060	42,385	42,273
Resolution range (Å)	32.7–1.50 (1.53–1.50)		27.2–1.50 (1.53–1.50)		
Completeness (%)	100 (100)	100 (99.9)	99.2 (93.3)	100 (100)	99.7 (99.6)
Multiplicity	400.1 (151.3)	36.3 (13.4)	12.4 (4.8)	439.4 (312.0)	12.9 (9.1)
R_{split} (%)[†]	7.8 (44.5)	24.4 (99.7)	43.1 (120.8)	7.1 (40.9)	41.4 (189.7)
$CC_{1/2}$	0.990 (0.776)	0.896 (0.389)	0.713 (0.272)	0.992 (0.810)	0.761 (0.124)
$<I/\sigma(I)>$	10.2 (2.3)	3.7 (1.3)	2.5 (1.5)	10.9 (2.8)	2.3 (0.9)
Total amounts of protein used (mg)	0.9	0.09	0.03	0.4	0.01
Refinement					
R/R_{free} (%)	17.6/19.3				
R.m.s. deviations					
Bond lengths (Å)	0.009				
Bond angles (°)	1.004				
PDB code	5wrc				

Table 1. Crystallographic statistics. Values in parentheses are for the outermost shell. [†]$R_{split} = 1/\sqrt{2} \frac{\sum_{hkl} |I_{even} - I_{odd}|}{1/2 \sum_{hkl} |I_{even} + I_{odd}|}$.
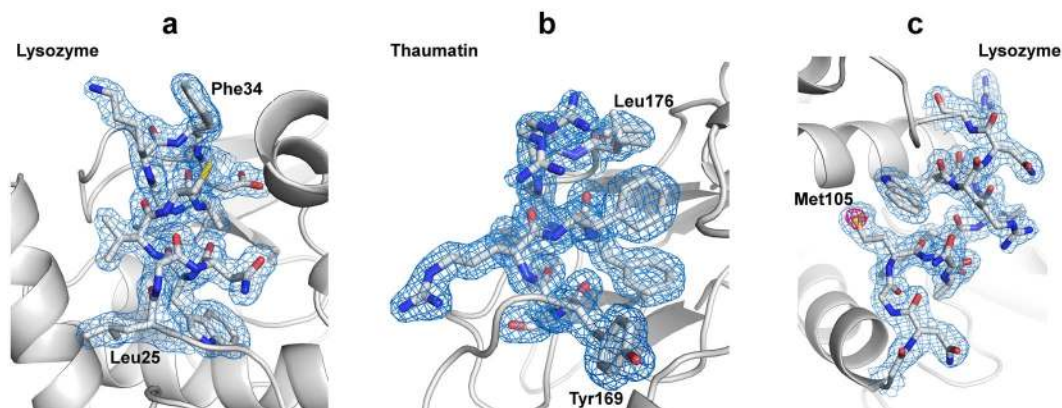
Figure 1. Electron density maps of lysozyme and thaumatin. Close-up views of (**a**) the lysozyme structure at 1.8-Å resolution and (**b**) the thaumatin structure at 1.55-Å resolution for the sample delivered in a cellulose matrix and (**c**) the lysozyme structure at 2.0-Å resolution for the sample delivered in a nuclear grease matrix with $2F_o - F_c$ electron density maps contoured at the $1.0\,\sigma$ level (coloured blue). An anomalous difference Fourier map contoured at the $4.0\,\sigma$ level (coloured magenta) shows the sulfur atom of Met105 in (**c**). These figures were drawn with PyMol (http://www.pymol.org).
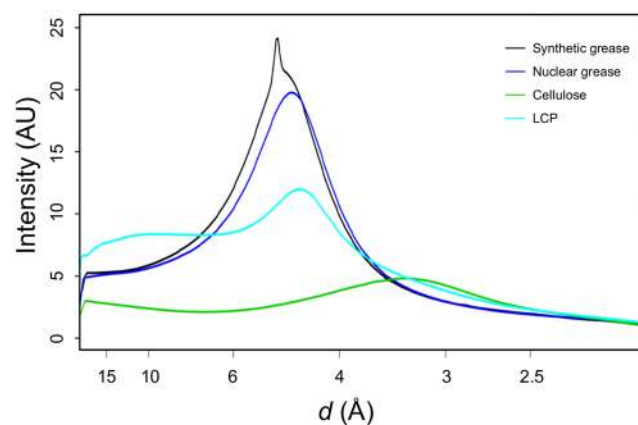

Figure 2. The average background scattering intensities of ~2,000 images from each matrix. Super Lube synthetic grease, Super Lube nuclear grease, 16% (*w/v*) hydroxyethyl cellulose solution and LCP are depicted by the black, blue, green and cyan lines, respectively.

Next, we employed single-isomorphous replacement (SIR) and SIR with anomalous scattering (SIRAS) for phasing. We obtained a data set (32,000 indexed images) from native crystals of proteinase K at a wavelength 0.95 Å[36], at a different beam time using different crystallization batches, at 1.5-Å resolution with a completeness of 100%, a $CC_{1/2}$ of 0.992. Only 2,000 images in total (native/derivative: 1,000/1,000) were sufficient for SIR and SIRAS phasing of proteinase K, while SAD phasing required 3,000 images. The $CC_{1/2}$ value of the 1,000-image derivative dataset was only 71.3% (27.2% for 1.53–1.50 Å), while that of the full dataset was 99.0% (77.6% for 1.53–1.50 Å) (Supplementary Fig. 4). As shown in Fig. 4, a combination of the native dataset with the derivative dataset boosted the peak heights in the anomalous difference map and allowed phasing from fewer images than using derivative images alone. This is in good agreement with the result from the previously reported I-SAD phasing of a membrane protein bacteriorhodopsin using an iododetergent[37].

In SFX, *de novo* phasing for heavy atom-derivatized proteions has been demonstrated[16, 37–42]. In addition, native sulfur SAD phasing was also achieved[40, 43, 44]. These results indicate that *de novo* phasing is now routinely available for SFX. Our cellulose matrix with low background scattering noise is compatible with the accurate measurement of weak anomalous signals essential for *de novo* phasing from SFX data.

A novel grease matrix with low background scattering. To reduce background scattering from conventional grease matrix[21, 26], we introduced a novel grease matrix, Super Lube nuclear grade approved grease (nuclear grease). For lysozyme crystals ($5 \times 5 \times 5\,\mu m$), we were able to collect ~100,000 images in approximately 1 hour at a wavelength 1.77 Å (Table 1). We indexed and integrated ~19,000 images for the lysozyme crystals. The crystals yielded data sets at 2.0-Å resolution with a completeness of 100% and a $CC_{1/2}$ of 0.988. We determined and refined the crystal structure of lysozyme (PDB ID: 5wrb) at 2.0-Å resolution.
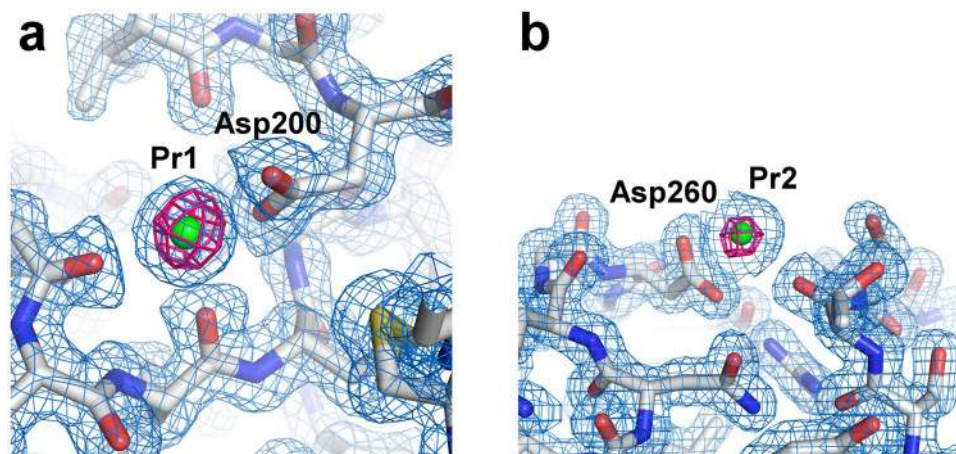
Figure 3. Electron density maps of proteinase K. (**a,b**) Close-up views of Pr ion binding sites with $2F_o − F_c$ electron density maps contoured at the $1.0\,\sigma$ level (coloured blue). Bound Pr ions are depicted as a green sphere. The anomalous difference Fourier maps using 3,000 images (contoured at the 6.0σ level) are shown in magenta. These figures were drawn with PyMol (http://www.pymol.org).
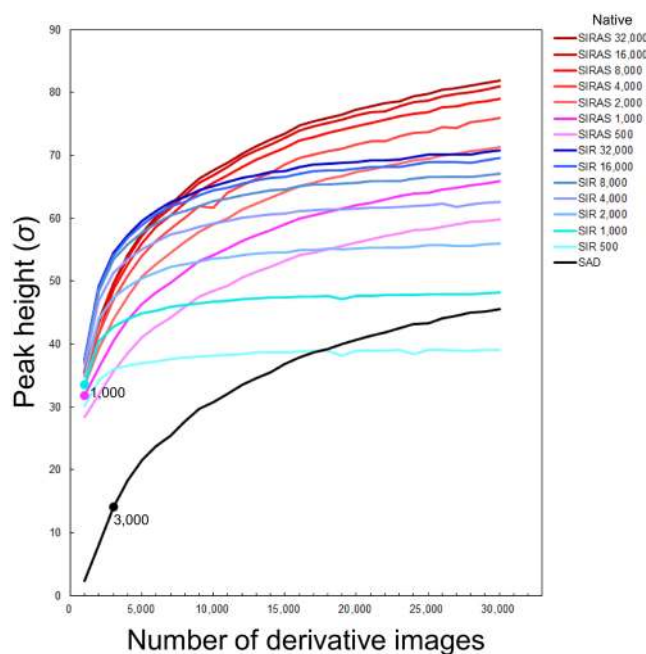
Figure 4. Improvement of anomalous difference peak heights with the number of derivative images. The plot of the sum of the anomalous peak heights from two Pr atoms. SAD, SIR and SIRAS phasing are shown in the black, blue and red lines, respectively. For SIR and SIRAS phasing, the number of native images were varied from 500 to 32,000. Filled circles indicate the minimum number of derivative images necessary for each phasing method and number of native images.

The conventional grease matrices (mineral-oil based AZ grease and untreated Super Lube synthetic grease without grinding treatment) extruded through a 110-μm-i.d. nozzle tended to produce a larger-diameter grease column (approximately ~210 μm) about the size of the outer diameter (o.d.) of the nozzle[21, 26]. On the other hand, the nuclear grease matrix was extruded as a continuous column with a diameter of ~100 μm through a 100-μm-i.d. nozzle (Supplementary Fig. 2b). The Super Lube synthetic grease tended to give a stronger diffraction ring at ~4.8-Å resolution in about 30% of all diffraction images (Fig. 2 and Supplementary Fig. 3b)[26]. Weaker background scattering was noted when using nuclear grease compared with Super Lube synthetic grease (Fig. 2 and Supplementary Fig. 3c). In the lysozyme structure with the nuclear grease matrix, we observed a weak anomalous scattering signal from sulfur atoms (e.g. the sulfur atom of Met105, Fig. 1c). On the other hand, an anomalous signal from the sulfur atoms in the proteinase K structure from ~20,000 indexed images was not discernible when using the conventional Super Lube synthetic grease matrix[26]. Using a wide variety of proteins, the adaptability of grease matrix has been demonstrated in SFX[15, 16, 18, 21, 26, 37, 39, 43, 45]. These results suggest that grease has

Media	Advantages	Disadvantages	References
Oil	general versatility	higher background scattering	
Nuclear grade grease	lower background scattering among grease matrices	salt-like impurities in grease	this study
Synthetic grease	higher versatility	gives a stronger diffraction ring at ~4.8 Å	26
Mineral-oil based grease	higher versatility	a larger diameter sample column	21
Vaseline (petroleum jelly)	a smaller diameter sample column (~40 μm)	gives stronger diffraction rings at 4.2 and 3.8 Å	22
Hydrogel	lower background scattering	damage to crystals by osmotic shock	
Hydroxyethyl cellulose	simple preparation	adhesive	this study
Hyaluronic acid	simple preparation	strongly adhesive, expensive	26
Agarose	compatible with proteins	requires heat treatment at temperatures higher than 85 °C as a pre-preparation	23
Other			
LCP (e.g., monoolein)	applicable to soluble and membrane proteins	higher background scattering, but lower than grease in the resolution range of 4–5 Å	20, 22, 23

Table 2. Crystal carrier media for serial sample loading.

potential as a versatile matrix carrier, but some crystals are incompatible with the grease matrix. The cellulose and hyaluronic acid matrices provide alternatives for grease-sensitive protein crystals. Grease and hydrogel crystal carriers are thus complementary (Table 2).

Using the cellulose matrix as a general protein carrier, we obtained the structures of soluble proteins beyond 1.8-Å resolution at room temperature. We have successfully applied Pr-SAD, SIR and SIRAS phasing to SFX, using 3,000 indexed images for SAD and 2,000 images for SIR and SIRAS, demonstrating that we can accurately measure anomalous signals. Matrix carriers with a stable sample flow and a small diameter sample column have various application in SFX experiments such as femtosecond to millisecond time-resolved studies of light-driven structural changes, and chemical dynamics using pump-probe techniques[14, 18, 46–50].

Materials and Methods

Sample preparation. Using a 20 mg ml^{-1} lysozyme solution, the crystals with a size of $1 \times 1 \times 1\,\mu$m, $5 \times 5 \times 5\,\mu$m and $20 \times 20 \times 30\,\mu$m were prepared following previously reported protocols[21], except for the incubation temperature during crystallization at 12, 17 and 26 °C for 10 min, respectively. Thaumatin I was purified from crude thaumatin powder as described previously[51]. Thaumatin crystallization was performed using the batch method. Microcrystals ($2 \times 2 \times 4\,\mu$m) were obtained by mixing in an ice bath an equal volume of the 40 mg ml^{-1} protein solutions and the reservoir solution, which consisted of 20 mM N-(2-acetamido) iminodiacetic acid (ADA) and 2.0 M potassium sodium tartrate (pH 7.3). Proteinase K from *Engyodontium album* (No. P2308, Sigma) at a concentration of 40 mg ml^{-1} was crystalized by previously reported protocols[26]. For Pr-derivatized proteinase K, a 100 μl sample of the crystal solution was added to a 100 μl heavy-atom solution comprised of 50 mM PrCl$_3$, 0.5 M NaNO$_3$ and 50 mM MES–NaOH (pH 6.5). The solution was then incubated at 20 °C for 90 min. To determine a crystal number density of the crystal solution, we counted the number of crystals in the solution using a hemocytometer (OneCell, cat. no. OC-C-S02) under a Hirox digital microscope (Hirox, KH-8700). The crystal number density was adjust to an approximately 10^7–10^8 crystals ml^{-1}.

In this study, we used hydroxyethyl cellulose (mw ~250,000, No. 09368, Sigma) as the crystal carrier matrix. Protein microcrystals were prepared according to the following procedures. For lysozyme and proteinase K crystals, after a 100-μl sample of storage solution was centrifuged at ~1,300–3,000 × g for 10 sec using a compact tabletop centrifuge, a 40-μl aliquot of supernatant solution was dispensed into 50 μl of 32% (w/v) hydroxyethyl cellulose aqueous solution for lysozyme ($1 \times 1 \times 1\,\mu$m) and proteinase K, or 22% (w/v) hydroxyethyl cellulose aqueous solution for lysozyme ($20 \times 20 \times 30\,\mu$m) on a glass slide and then mixed with a spatula for ~15 sec. After a 50-μl aliquot of the remaining supernatant solution was removed, a 10-μl aliquot of the crystal solution was dispensed into 90 μl of the hydroxyethyl cellulose solution and then mixed for ~15 sec. For thaumatin crystals, after a 100-μl sample of storage solution was centrifuged at ~1,300–3,000 × g for 10 sec using a compact tabletop centrifuge, a 90-μl aliquot of supernatant solution was removed. A 10-μl aliquot of the crystal solution was dispensed into 90 μl of 24% (w/v) hydroxyethyl cellulose aqueous solution on a glass slide and then mixed for ~15 sec. For the grease matrix, the lysozyme crystals ($5 \times 5 \times 5\,\mu$m) were mixed with the Super Lube nuclear grade grease (No. 42150, Synco Chemical Co.) using the same procedure reported by Sugahara *et al.*[21] The grease was filtered through 10 μm mesh (No. 06-04-0041-2314, CellTrics) before mixing with protein crystals to remove salt-like impurities in the grease. We performed this matrix preparation immediately before SFX experiments.

Data collection. We carried out the experiments using femtosecond X-ray pulses from SACLA[27]. The X-ray wavelength was 0.95, 1.24 or 1.77 Å (13, 10 or 7 keV) with a pulse energy of ~200 μJ. Each X-ray pulse delivers

ture.com/scientificreports/

$\sim 7 \times 10^{10}$ photons within a 10-fs duration (FWHM) at a wavelength of 1.77 Å (7 keV) to the matrices. Data were collected using focused X-ray beams of $1.5 \times 1.5 \mu m^2$ by Kirkpatrick-Baez mirrors[52]. The crystals in a cellulose or grease matrix were serially loaded using a high viscosity micro-extrusion injector system installed in a helium ambiance, diffraction chamber. The experiments were carried out using a Diverse Application Platform for Hard X-ray Diffraction in SACLA (DAPHNIS)[28] at BL3[53]. The microcrystals embedded in the matrix were kept at a temperature of approximately 20 °C in the micro-extrusion injector. The sample chamber was kept at a temperature of ~26 °C and a humidity greater than 50%. Diffraction images were collected using a custom-built 4M pixel detector with multi-port CCD sensors[54]. The matrix with randomly oriented crystals was extruded through injector nozzles with inner diameters (i.d.) of 50, 100, 110 or 130 μm (Table 1). Data collection was guided by realtime analysis by the SACLA data processing pipeline[55].

Background intensity determination. The background intensities from Super Lube synthetic grease, Super Lube nuclear grease and hydroxyethyl cellulose through a 100-μm-i.d. nozzle at 1.77 Å and that from LCP[14] through a 75-μm-i.d. nozzle at 1.61 Å were determined by a procedure similar to that used in Conrad *et al.*[23] Details of the calculation have been described previously[26]. Diffraction images for LCP were retrieved from CXIDB[56] (http://www.cxidb.org/) #53.

Structure determination. Diffraction images were filtered and converted by *Cheetah*[57] adapted[55] for the SACLA data acquisition system[58]. Diffraction peak positions were determined using the built-in Zaefferer algorithm and passed on to *DirAx*[59] for indexing. No sigma cutoff or saturation cutoff were applied. Measured diffraction intensities were merged by *process_hkl* in the *CrystFEL* suite[60] with scaling (–*scale* option). The structures of lysozyme and thaumatin were determined by difference Fourier synthesis using search models (PDB: 3WUL for lysozyme, and 3X3P for thaumatin). For Pr-derivatized proteinase K, substructure search, phasing and phase improvement were carried out using the *SHELX C, D* and *E* programs[30]. The autotraced model from *SHELXE* was fed into *Buccaneer*[32] from the *CCP4* suite[61]. Manual model revision and structure refinement were performed using *Coot*[62] and *PHENIX*[63], respectively. Details of the data collection and refinement statistics are summarized in Table 1.

References

1. Chapman, H. N. *et al.* Femtosecond X-ray protein nanocrystallography. *Nature* **470**, 73–77, doi:10.1038/nature09750 (2011).
2. Neutze, R., Wouts, R., van der Spoel, D., Weckert, E. & Hajdu, J. Potential for biomolecular imaging with femtosecond X-ray pulses. *Nature* **406**, 752–757, doi:10.1038/35021099 (2000).
3. Emma, P. *et al.* First lasing and operation of an ångstrom-wavelength free-electron laser. *Nat. Photonics* **4**, 641–647, doi:10.1038/nphoton.2010.176 (2010).
4. Schlichting, I. & Miao, J. Emerging opportunities in structural biology with X-ray free-electron lasers. *J. Curr. Opin. Struct. Biol.* **22**, 613–626, doi:10.1016/j.sbi.2012.07.015 (2012).
5. Barty, A. *et al.* Self-terminating diffraction gates femtosecond X-ray nanocrystallography measurements. *Nat. Photonics* **6**, 35–40, doi:10.1038/nphoton.2011.297 (2012).
6. Schlichting, I. Serial femtosecond crystallography: the first five years. *IUCrJ* **2**, 246–255, doi:10.1107/S205225251402702X (2015).
7. Fukuda, Y. *et al.* Redox-coupled structural changes in nitrite reductase revealed by serial femtosecond and microfocus crystallography. *J. Biochem.* **159**, 527–538, doi:10.1093/jb/mvv133 (2016).
8. Johansson, L. C. *et al.* Lipidic phase membrane protein serial femtosecond crystallography. *Nat. Methods* **9**, 263–265, doi:10.1038/nmeth.1867 (2012).
9. Redecke, L. *et al.* Natively inhibited Trypanosoma brucei cathepsin B structure determined by using an X-ray laser. *Science* **339**, 227–230, doi:10.1126/science.1229663 (2013).
10. Liu, W. *et al.* Serial femtosecond crystallography of G protein–coupled receptors. *Science* **342**, 1521–1524, doi:10.1126/science.1244142 (2013).
11. Kang, Y. *et al.* Crystal structure of rhodopsin bound to arrestin by femtosecond X-ray laser. *Nature* **523**, 561–567, doi:10.1038/nature14656 (2015).
12. Zhang, H. *et al.* Structure of the Angiotensin receptor revealed by serial femtosecond crystallography. *Cell* **161**, 833–844, doi:10.1016/j.cell.2015.04.011 (2015).
13. Zhou, Q. *et al.* Architecture of the synaptotagmin–SNARE machinery for neuronal exocytosis. *Nature* **525**, 62–67, doi:10.1038/nature14975 (2015).
14. Nango, E. *et al.* A three dimensional movie of structural changes in bacteriorhodopsin. *Science* **354**, 1552–1557, doi:10.1126/science.aah3497 (2016).
15. Colletier, J. P. *et al.* Serial Femtosecond Crystallography and Ultrafast Absorption Spectroscopy of the Photoswitchable Fluorescent Protein IrisFP. *J. Phys. Chem. Lett.* **7**, 882–887, doi:10.1021/acs.jpclett.5b02789 (2016).
16. Fukuda, Y. *et al.* Redox-coupled proton transfer mechanism in nitrite reductase revealed by femtosecond crystallography. *Proc. Natl. Acad. Sci. USA* **113**, 2928–2933, doi:10.1073/pnas.1517770113 (2016).
17. Stagno, J. R. *et al.* Structures of riboswitch RNA reaction states by mix-and-inject XFEL serial crystallography. *Nature* **541**, 242–246, doi:10.1038/nature20599 (2017).
18. Suga, M. *et al.* Light-induced structural changes and the site of O=O bond formation in PSII caught by XFEL. *Nature* **543**, 131–135, doi:10.1038/nature21400 (2017).
19. DePonte, D. P. *et al.* Gas dynamic virtual nozzle for generation of microscopic droplet streams. *J. Phys. D Appl. Phys.* **41**, 195505, doi:10.1088/0022-3727/41/19/195505 (2008).
20. Weierstall, U. *et al.* Lipidic cubic phase injector facilitates membrane protein serial femtosecond crystallography. *Nat. Commun.* **5**, 3309, doi:10.1038/ncomms4309 (2014).
21. Sugahara, M. *et al.* Grease matrix as a versatile carrier of proteins for serial crystallography. *Nat. Methods* **12**, 61–63, doi:10.1038/nmeth.3172 (2015).
22. Botha, S. *et al.* Room-temperature serial crystallography at synchrotron X-ray sources using slowly flowing free-standing high-viscosity microstreams. *Acta Cryst.* **D71**, 387–397, doi:10.1107/S1399004714026327 (2015).
23. Conrad, C. E. *et al.* A novel inert crystal delivery medium for serial femtosecond crystallography. *IUCrJ* **2**, 421–430, doi:10.1107/S2052252515009811 (2015).
24. Stellato, F. *et al.* Room-temperature macromolecular serial crystallography using synchrotron radiation. *IUCrJ* **1**, 204–212, doi:10.1107/S2052252514010070 (2014).

25. Nogly, P. *et al*. Lipidic cubic phase serial millisecond crystallography using synchrotron radiation. *IUCrJ* **2**, 168–176, doi:10.1107/S2052252514026487 (2015).

26. Sugahara, M. *et al*. Oil-free hyaluronic acid matrix for serial femtosecond crystallography. *Sci. Rep.* **6**, 24484, doi:10.1038/srep24484 (2016).

27. Ishikawa, T. *et al*. A compact X-ray free-electron laser emitting in the sub-ångström region. *Nat. Photonics* **6**, 540–544, doi:10.1038/nphoton.2012.141 (2012).

28. Tono, K. *et al*. Diverse application platform for hard X-ray diffraction in SACLA (DAPHNIS): application to serial protein crystallography using an X-ray free-electron laser. *J. Synchrotron Rad.* **22**, 532–537, doi:10.1107/S1600577515004464 (2015).

29. Cheng, A., Hummel, B., Qiu, H. & Caffrey, M. A simple mechanical mixer for small viscous lipid-containing samples. *Chem. Phys. Lipids* **95**, 11–21, doi:10.1016/S0009-3084(98)00060-7 (1998).

30. Sheldrick, G. M. Experimental phasing with SHELXC/D/E: combining chain tracing with density modification. *Acta Cryst.* **D66**, 479–485, doi:10.1107/S0907444909038360 (2010).

31. Yazawa, K. *et al*. Derivatization of Proteinase K with Heavy Atoms Enhances Its Thermal Stability. *ACS Catalysis* **6**, 3036–3046, doi:10.1021/acscatal.6b00100 (2016).

32. Cowtan, K. The Buccaneer software for automated model building. 1. Tracing protein chains. *Acta Cryst.* **D62**, 1002–1011, doi:10.1107/S0907444906022116 (2006).

33. Hendrickson, W. A. & Teeter, M. M. Structure of the hydrophobic protein crambin determined directly from the anomalous scattering of sulphur. *Nature* **290**, 107–113, doi:10.1038/290107a0 (1981).

34. Dauter, Z., Dauter, M., de La Fortelle, E., Bricogne, G. & Sheldrick, G. M. Can anomalous signal of sulfur become a tool for solving protein crystal structures? *J. Mol. Biol.* **289**, 83–92, doi:10.1006/jmbi.1999.2743 (1999).

35. Thorn, A. & Sheldrick, G. M. ANODE: anomalous and heavy-atom density calculation. *J. Appl. Cryst.* **44**, 1285–1287, doi:10.1107/S0021889811041768 (2011).

36. Masuda, T. *et al*. Atomic resolution structure of serine protease proteinase K at ambient temperature. *Sci. Rep.* **7**, 45604, doi:10.1038/srep45604 (2017) (*in press*).

37. Nakane, T. *et al*. Membrane protein structure determination by SAD, SIR or SIRAS phasing in serial femtosecond crystallography using a novel iododetergent. *Proc. Natl. Acad. Sci. USA* **113**, 13039–13044, doi:10.1073/pnas.1602531113 (2016).

38. Barends, T. R. M. *et al*. *De novo* protein crystal structure determination from X-ray free-electron laser data. *Nature* **505**, 244–247, doi:10.1038/nature12773 (2014).

39. Yamashita, K. *et al*. An isomorphous replacement method for efficient *de novo* phasing for serial femtosecond crystallography. *Sci. Rep*. **5**, 14017, doi:10.1038/srep14017 (2015).

40. Nass, K. *et al*. Protein structure determination by single-wavelength anomalous diffraction phasing of X-ray free-electron laser data. *IUCrJ* **3**, 180–191, doi:10.1107/S2052252516002980 (2016).

41. Colletier, J. P. *et al*. *De novo* phasing with X-ray laser reveals mosquito larvicide BinAB structure. *Nature* **539**, 43–47, doi:10.1038/nature19825 (2016).

42. Hunter, M. S. *et al*. Selenium single-wavelength anomalous diffraction *de novo* phasing using an X-ray-free electron laser. *Nat. Commun.* **7**, 13388, doi:10.1038/ncomms13388 (2016).

43. Nakane, T. *et al*. Native sulfur/chlorine SAD phasing for serial femtosecond crystallography. *Acta Cryst*. **D71**, 2519–2525, doi:10.1107/S139900471501857X (2015).

44. Batyuk, A. *et al*. Native phasing of x-ray free-electron laser data for a G protein–coupled receptor. *Sci. Adv.* **2**, e1600292, doi:10.1126/sciadv.1600292 (2016).

45. Edlund, P. *et al*. The room temperature crystal structure of a bacterial phytochrome determined by serial femtosecond crystallography. *Sci. Rep.* **6**, 35279, doi:10.1038/srep35279 (2016).

46. Nogly, P. *et al*. Lipidic cubic phase injector is a viable crystal delivery system for time-resolved serial crystallography. *Nat. Commun*. **7**, 12314, doi:10.1038/ncomms12314 (2016).

47. Barends, T. R. M. *et al*. Direct observation of ultrafast collective motions in CO myoglobin upon ligand dissociation. *Science* **350**, 445–450, doi:10.1126/science.aac5492 (2015).

48. Kern, J. *et al*. Taking snapshots of photosynthetic water oxidation using femtosecond X-ray diffraction and spectroscopy. *Nat. Commun.* **5**, 4371, doi:10.1038/ncomms5371 (2014).

49. Kupitz, C. *et al*. Serial time-resolved crystallography of photosystem II using a femtosecond X-ray laser. *Nature* **513**, 261–265, doi:10.1038/nature13453 (2014).

50. Tenboer, J. *et al*. Time-resolved serial crystallography captures high-resolution intermediates of photoactive yellow protein. *Science* **346**, 1242–1246, doi:10.1126/science.1259357 (2014).

51. Masuda, T., Ohta, K., Mikami, B. & Kitabatake, N. High-resolution structure of the recombinant sweet-tasting protein thaumatin I. *Acta Cryst*. **F67**, 652–658, doi:10.1107/S174430911101373X (2011).

52. Yumoto, H. *et al*. Focusing of X-ray free-electron laser pulses with reflective optics. *Nat. Photonics* **7**, 43–47, doi:10.1038/nphoton.2012.306 (2013).

53. Tono, K. *et al*. Beamline, experimental stations and photon beam diagnostics for the hard x-ray free electron laser of SACLA. *New J. Phys*. **15**, 083035, doi:10.1088/1367-2630/15/8/083035 (2013).

54. Kameshima, T. *et al*. Development of an X-ray pixel detector with multi-port charge-coupled device for X-ray free-electron laser experiments. *Rev. Sci. Instrum*. **85**, 033110, doi:10.1063/1.4867668 (2014).

55. Nakane, T. *et al*. Data processing pipeline for serial femtosecond crystallography at SACLA. *J. Appl. Cryst*. **49**, 1035–1041, doi:10.1107/S1600576716005720 (2016).

56. Maia, F. R. N. C. The Coherent X-ray Imaging Data Bank. *Nat. Methods* **9**, 854–855, doi:10.1038/nmeth.2110 (2012).

57. Barty, A. *et al*. Cheetah: software for high-throughput reduction and analysis of serial femtosecond X-ray diffraction data. *J. Appl. Cryst.* **47**, 1118–1131, doi:10.1107/S1600576714007626 (2014).

58. Joti, Y., Kameshima, T., Yamaga, M., Sugimoto, T. & Okada, K. Data acquisition system for X-ray free-electron laser experiments at SACLA. *J. Synchrotron Rad*. **22**, 571–576, doi:10.1107/S1600577515004506 (2015).

59. Duisenberg, A. J. M. Indexing in single-crystal diffractometry with an obstinate list of reflections. *J. Appl. Cryst.* **25**, 92–96, doi:10.1107/S0021889891010634 (1992).

60. White, T. A. *et al*. CrystFEL: a software suite for snapshot serial crystallography. *J. Appl. Cryst.* **45**, 335–341, doi:10.1107/S0021889812002312 (2012).

61. Collaborative Computational Project, Number 4. The CCP4 suite: programs for protein crystallography. *Acta Cryst.* **D50**, 760–763 (1994).

62. Emsley, P. & Cowtan, K. Coot: model-building tools for molecular graphics. *Acta Cryst.* **D60**, 2126–2132, doi:10.1107/S0907444904019158 (2004).

63. Adams, P. D. *et al*. PHENIX: a comprehensive Python-based system for macromolecular structure solution. *Acta Cryst.* **D66**, 213–221 (2010).

Acknowledgements

Author Contributions

Additional Information

Supplementary information accompanies this paper at doi:10.1038/s41598-017-00761-0

Accession codes: The coordinates and structure factors have been deposited in the Protein Data Bank under the accession code 5wr9, 5wra and 5wrb for lysozyme, 5wr8 for thaumatin and 5wrc for proteinase K. Diffraction images have been deposited to CXIDB under ID 45 (proteinase K, native), 48 (proteinase K, derivative), 49 (thaumatin) 47 (lysozyme, grease) and 50 (lysozyme, cellulose).